Available online at www.sciencedirect.com
SCIENCE DIRECT®
Polymer 44 (2003) 4363–4372
polymer
www.elsevier.com/locate/polymer

The molecular basis of CO_2 interaction with polymers containing fluorinated groups: computational chemistry of model compounds and molecular simulation of poly[bis(2,2,2-trifluoroethoxy)phosphazene]

J.R. Fried*, N. Hu

OBR Center for Computer-Aided Molecular Design, Department of Chemical and Materials Engineering, University of Cincinnati, Cincinnati, OH 45221-0012, USA

Received 4 February 2003; received in revised form 24 March 2003; accepted 24 March 2003

Abstract

Ab initio molecular orbital calculations of CO_2 and model compounds have been used to identify the nature of specific interactions between CO_2 and the fluorinated substituent groups of polymers such as poly(trifluoropropyl methyl siloxane) and poly[bis(2,2,2-trifluoroethoxy)phosphazene] (PTFEP) that exhibits high CO_2 permeability and permselectivity. Second-order Møller–Plesset (MP2) perturbation calculations (6-311++G^{**} basis set) were used to obtain energies, dipole and quadrupole moments, and polarizabilities of CO_2, three alkanes (CH_4, CH_3CH_3, and $CH_3CH_2CH_3$), and three fluoroalkanes (CF_4, CH_3CF_3, and $CH_3CH_2CF_3$). Results of energy calculations of three CO_2–alkane and three CO_2–fluoroalkane dimers indicate that CO_2 forms a favorable quadrupole–dipole interaction with the fluoroalkyl groups. The maximum quadrupole–dipole interaction energy obtained was -11.5 kJ mol^{-1} for CO_2–$CF_3CH_2CH_3$. This value is less than interaction energies typical for hydrogen bonding but greater than the London dispersion values reported for the interaction of CO_2 with the carbonyl group of poly(methyl methacrylate) (PMMA). Electrostatic potential distributions indicate a small redistribution of electron density to the fluorine atoms of the trifluoroalkanes and to the oxygen atoms of CO_2 in the CO_2–CF_3CH_3 and CO_2–$CF_3CH_2CH_3$ dimers.

Sorption and molecular association of CO_2 with PTFEP has been investigated by molecular simulation of an amorphous cell using the COMPASS molecular mechanics force field. CO_2 sorption isotherms obtained by Grand Canonical Monte Carlo (GCMC) simulation indicate an upward deviation from the linear relationship between log S and the Lennard–Jones potential well depth parameter, ε/k, in agreement with reported permeability data. Pair-correlation analysis obtained from molecular dynamics simulation show strong correlation of CO_2 with the trifluoromethyl group of PTFEP in agreement with the MP2 results showing an association of CO_2 with both CH_3CF_3 and $CH_3CH_2CF_3$.

Keywords: Carbon dioxide; Solubility; Molecular association

1. Introduction

It has been widely observed that many fluorinated compounds including simple fluorocarbons [1,2] and many fluorine-containing polymers such as vinylidene fluoride polymers [3] and perfluoropolymers including polytetrafluoroethylene [4] can be dissolved by supercritical CO_2 at high temperature and pressure. In addition, several studies have reported high solubility of CO_2 in some fluorine-containing polymers [5,6]. The basis for this behavior has been the subject of some speculation and interest due to the attractive permselectivity of these polymers for CO_2 in mixtures with other gases such as methane. Examples of polymers reported to exhibit enhanced CO_2 permeability include poly(trifluoropropyl methyl siloxane) (PTFPMS) [6], some fluorine-containing polycarbonates [7] and polyimides [8,9], poly(vinylidene fluoride) (PVDF) [10,11], poly[*o*-(trifluoromethyl)phenylacetylene] (TFMPA) [12], fluorine-containing norbornene polymers [13], and poly[bis(2,2,2-trifluoroethoxy)phosphazene] (PTFEP) [14]. Structures of these polymers are shown in Table 1 to illustrate the location of accessible fluorine sites.

* Corresponding author. Tel.: +1-513-556-3096; fax: +1-513-556-2569.
E-mail address: joel.fried@uc.edu (J.R. Fried).

0032-3861/03/$ - see front matter © 2003 Elsevier Science Ltd. All rights reserved.
doi:10.1016/S0032-3861(03)00285-4

Table 1
Structures of fluorine-containing polymers

Polymer	Structure
Poly(trifluoropropyl methyl siloxane) (PTFPMS)	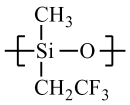
Poly[*o*-(trifluoromethyl)phenylacetylene] (PTFMPA)	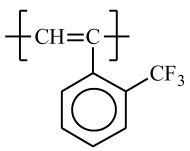
Tetramethylhexafluorobisphenol-A polycarbonate (TMHF-PC)	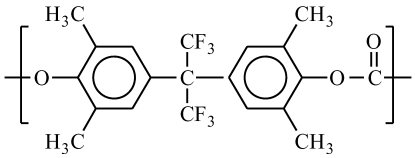
Hexafluorobisphenol-A polycarbonate (HFPC)	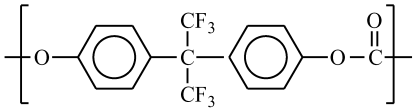
6FDA-4,4′-ODA[a] polyimide	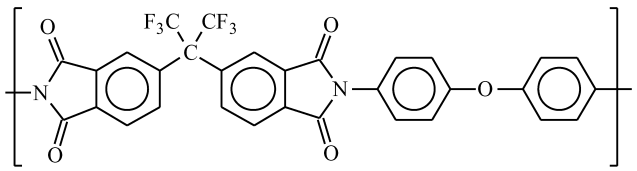
6FDA-DAF[b] polyimide	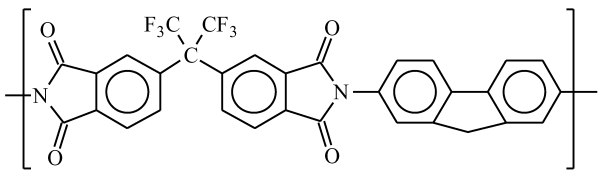
6FDA-BAHF[c] polyimide	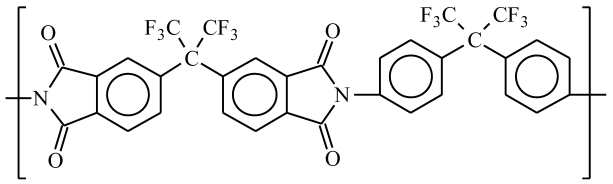
Poly[5,5-difluoro-6,6-bis(trifluoromethyl)-norbornene] (PFMNB)	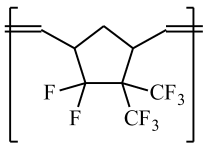
Poly(vinylidene fluoride) (PVDF)	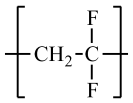
Poly[bis(2,2,2-trifluoroethoxy)phosphazene] (PTFEP)	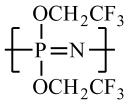

[a] ODA: 4,4-oxydianiline.
[b] DAF, diaminofluorene.
[c] 2,2-Bis(3,4-dicarboxyphenyl)hexafluoropropane dianhydride/2,2-bis(4-aminophenyl)hexafluoropropane.

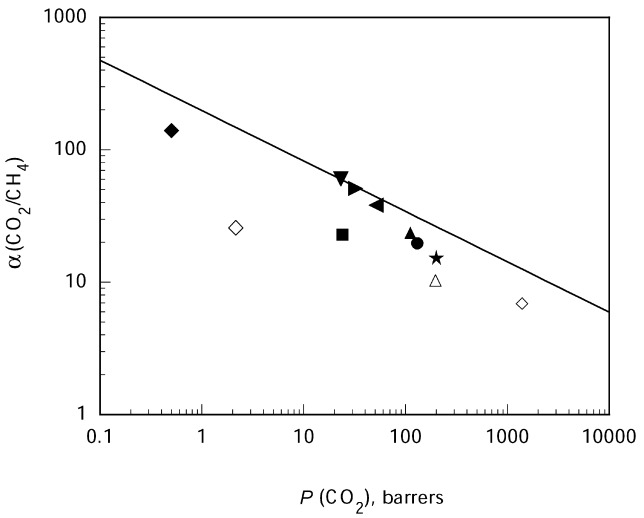

Fig. 1. Logarithmic plot of the ideal permselectivity of CO_2/CH_4 versus CO_2 permeability. Line represents Robeson [15] boundary. Data points for PTFEP (△), PTFMPA (●), PTFPMS (◇), HFPC (■), TMHF-PC (▲), PVDF (◇), 6FDA-ODA (▼), 6FDA-DAF (►), 6FDA-BAHF (◄), PMMA (◆), and PFMNB (★). Closed symbols represent glassy polymers; open symbols represent rubbery polymers. See Table 1 for polymer structures.

The potential of a given polymer for a particular separation, such as CO_2 from a mixture with CH_4, can be assessed from a plot of ideal permselectivity, the ratio of permeabilities of the two pure gases in the form

$$\alpha_{CO_2,CH_4} = \frac{P(CO_2)}{P(CH_4)} \quad (1)$$

versus permeability, $P(CO_2)$. Permselectivities of the fluorinated polymers cited previously are plotted against their CO_2 permeabilities in Fig. 1 and are compared to the Robeson [15] line delineating the upper boundary for CO_2/CH_4 given as

$$P_{CO_2}(\text{barrers}) = 1.0737 \times 10^6 (\alpha_{CO_2,CH_4})^{-2.6264} \quad (2)$$

This boundary marks the upper bound between CO_2/CH_4 permselectivity and CO_2 permeability for approximately 300 glassy and rubbery polymers reported in the literature. With the exception of PVDF, which is highly crystalline and has low permeability, the fluorine-containing polymers have CO_2 permeabilities and permselectivities close to the boundary.

Stern and co-workers [5,6] has attributed the high solubility of CO_2 in simple fluoroalkane-substituted polymers such as PTFPMS, to a 'specific interaction' between CO_2 and the polar fluoroalkane groups of this polymer. In the case of poly(organophosphazenes), PTFEP exhibits the highest reported CO_2/CH_4 permselectivity [16]. The high solubility of CO_2 in PTFEP has been attributed to interactions between CO_2 and the electron-withdrawing trifluoroethoxy group [14,17].

In the absence of specific interactions, the solubility of fixed gases can be correlated with various measures of the condensability [18] of the gas such as the critical temperature [5], boiling point [12], or the Lennard–Jones potential well-depth parameter, ε/k, [10] in the form [19,20] of

$$\log S = \log S^0 + m(\varepsilon/k) \quad (3)$$

As an approximation, the slope m is independent of the nature of the sorbing medium and is in the order of $10^{-2}\ K^{-1}$. In a study by Hirose et al. [14], CO_2 solubility in PTFEP was found to be significantly higher than would be expected on the basis of this correlation. Similar observations were reported by Starannikova et al. [17] in a study of two PTFEP samples having different crystallinity. The elevated solubility of CO_2 in PTFEP is shown in Fig. 2 where log S is plotted against ε/k. Similar behavior is shown in Fig. 2 for PTFPMS and the fluorine-containing polynorbornene, PFMNB (see Table 1 for structures).

Since fluoroalkanes have high polarity and CO_2 is known to have a large quadrupole moment [21] as a result of its highly electronegative oxygen atoms, it is probable that the favorable interaction suggested by the solubility data may be due to a quadrupole–dipole interaction between CO_2 and the fluoroalkyl (or fluoroalkoxy) groups. In the first part of this study, dipole and quadrupole moments of CO_2, three alkanes (CH_4, CH_3CH_3, and $CH_3CH_2CH_3$), and three fluoroalkanes (CF_4, CH_3CF_3, and $CH_3CH_2CF_3$) have been calculated using second-order Møller–Plesset perturbation (MP2) theory [22] and the 6-311++G** basis set to incorporate electron correlation effects. In addition, total energies of CO_2 complexes with each of the alkanes and fluoroalkanes have been obtained from MP2/6-311++G** calculations and the relative contributions of dipole and quadrupole interactions have been identified.

Molecular simulations have been used to investigate the

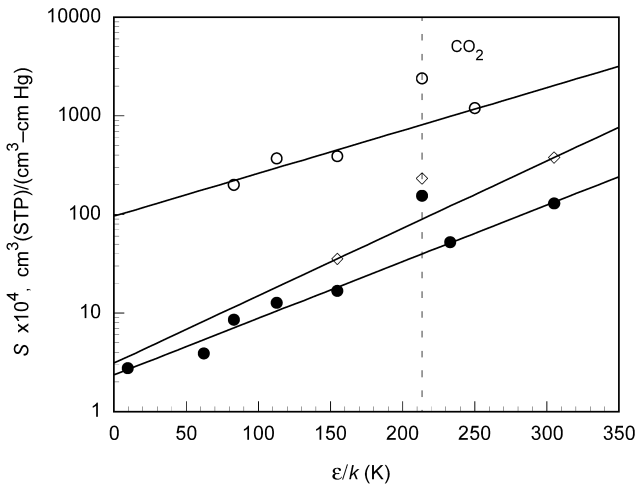

Fig. 2. Semilogarithmic plot of gas solubility versus the Lennard–Jones potential well-depth parameters, ε/k. Solubility data: PTFEP (●), Hirose et al. [14]; PTMPS (◇), Stern et al. [6]; PFMNB (○), Yampol'skii et al. [13]. Values of Lennard–Jones potential well-depth parameters were taken from Teplyakov and Meares [20]. Lines are drawn by least-square fit of experimental data with the exclusion of the CO_2 data point. Broken vertical line locates experimental solubility data for CO_2.

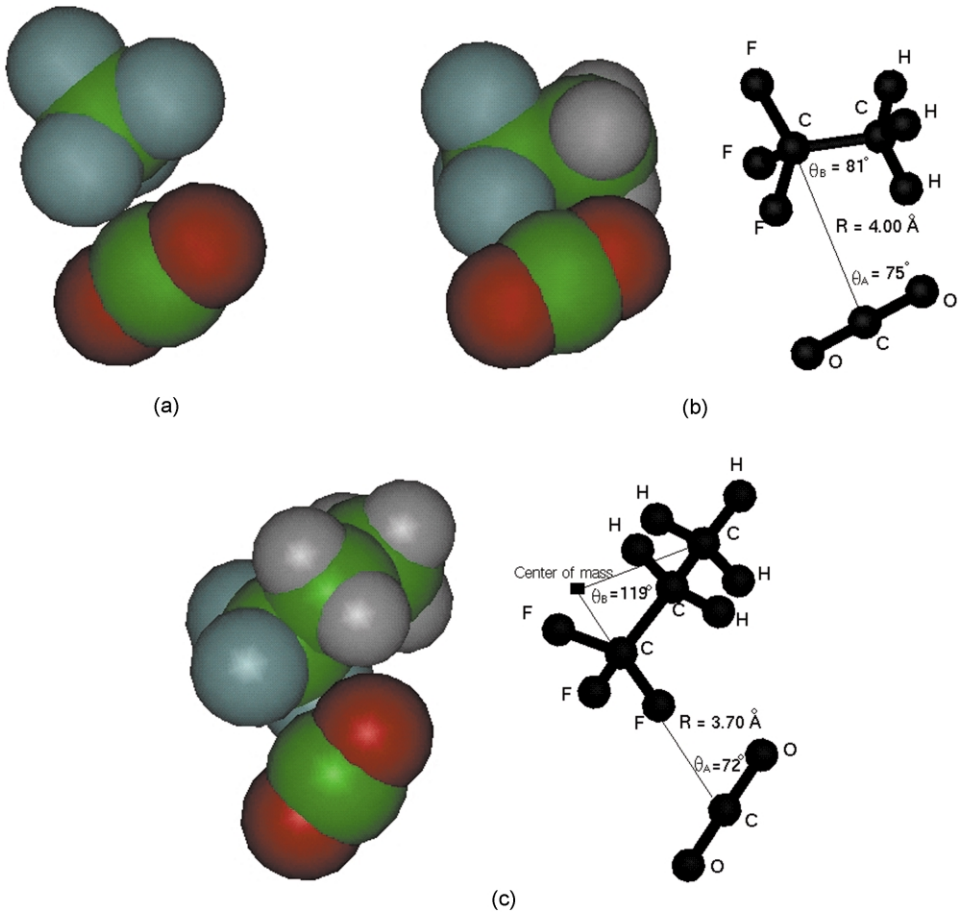

Fig. 3. (a) Space filling model showing energetically favorable interaction of CO_2 with tetrafluoromethane; (b) space filling and ball and stick representations of CO_2 interaction with trifluoroethane; (c) space filling and ball-and-stick representations of CO_2 interaction with trifluoropropane.

interaction of CO_2 with the fluoroethoxy group of PTFEP. Grand Canonical Monte Carlo (GCMC) simulation has been used to obtain solubility coefficients of He, N_2, O_2, CH_4, CO_2, and Xe; molecular dynamics has been used to investigate the association of CO_2 with the different atom positions and substituent groups of PTFEP by analysis of pair correlation functions. The force field used in these simulations is condensed-phase optimized molecular potentials for atomistic simulation studies (COMPASS) [23]. COMPASS is a class II ab initio force field that includes extensive use of cross terms and a 6–9 Lennard–Jones potential and a Coulombic expression for nonbonded terms. Details of individual force field terms in COMPASS have been given in earlier publications [23,24]. COMPASS has been parameterized and validated for polysilanes [25], alkanes and benzene compounds [23], and a variety of inorganic compounds and fixed gases [26]. Of particular importance to the present study, COMPASS has been extensively parameterized and validated for phosphazenes and polyorganophosphazenes [24] and has been successively used to simulate the glass transition [27] and gas diffusion and solubility [28] of poly[bis(butoxyphosphazenes)].

2. Computational background

The elements of the quadrupole moment tensor were obtained as [29]

$$Q_{ij} = \int \sigma(\mathbf{r}) r_i r_j \, \mathrm{d}\mathbf{r} \tag{4}$$

where $\sigma(\mathbf{r})$ is the charge density distribution and r_i and r_j are the components of the distance vector from the molecular center. With CO_2 oriented along the x-axis and the carbon atom positioned at the origin, the off-diagonal elements become zero and the quadrupole moment is obtained as

$$\boldsymbol{\Theta} = Q_{zz} - Q_{xx} \tag{5}$$

Polarizability was calculated as the average of the diagonal components of the polarizability tensor as

$$\alpha = \frac{1}{3}(\alpha_{xx} + \alpha_{yy} + \alpha_{zz}) \tag{6}$$

Dipole–quadrupole and quadrupole–quadrupole interaction energies were calculated from values of the dipole and quadrupole moments and the orientation angles, θ and

ϕ, (see Fig. 3(b) and (c)) according to the equations [30]

$$U_{\mu\Theta} = \frac{\mu_A \Theta_B}{4\pi\varepsilon_0 R^4}\frac{3}{2}[\cos\theta_A(3\cos^2\theta_B - 1) - 2\sin\theta_A \times \sin\theta_B \cos\theta_B \cos\phi] \quad (7)$$

and

$$U_{\Theta\Theta} = \frac{\Theta_A \Theta_B}{4\pi\varepsilon_0 R^5}\frac{3}{4}[1 - 5\cos^2\theta_A - 5\cos^2\theta_B - 15\cos^2\theta_A\cos^2\theta_B + 2(4\cos\theta_A\cos\theta_B - \sin\theta_A \sin\theta_B\cos\phi)^2] \quad (8)$$

where ε_0 is the dielectric permittivity of free space (8.854×10^{-12} C^2 J^{-1} m^{-1}) and R is the distance between the centers of mass of the two interacting molecules as shown in Fig. 3(b) and (c).

The pair correlation coefficient (PCF), $g_{\alpha\beta}(r)$, provides a measure of the probability that, given the presence of an atom at the origin of an arbitrary reference frame, there will be an atom with its center located in a spherical shell of infinitesimal thickness at a distance r from the reference atom.

The solubility coefficients, S, were obtained from GCMC simulation of the sorption isotherms. In this procedure, a Metropolis [31] algorithm is used to accept or reject a configurational move (rotation and translation) and an insertion and deletion of a sorbate molecule. The configurational move is accepted if the energy change, ΔU, is negative or if the Boltzmann factor, $\exp(-\Delta U/kT)$ is greater than a random number generated between 0 and 1. Formally, the probability, P, of a move being accepted is expressed as

$$P = \min\left[1; \exp\left(\frac{-\Delta U}{kT}\right)\right]$$

where U is calculated from the sum of nonbonded (i.e. Coulombic and van der Waals interaction) energies. Similarly, the probabilities for addition and deletion of a sorbate molecule are given as

$$P_{add} = \min\left[1; \frac{1}{N+1}\frac{pV}{kT}\exp\left(\frac{-\Delta U}{kT}\right)\right]$$

and

$$P_{del} = \min\left[1; \frac{NkT}{pV}\exp\left(\frac{-\Delta U}{kT}\right)\right]$$

respectively, where N is the number of sorbate molecules. The solubility coefficient, S, is then obtained from the slope of the sorption isotherm as

$$S = \lim_{p\to 0}\frac{c}{p} \quad (9)$$

where c is the sorbed gas concentration, units of cm^3(STP)/cm^3 polymer, and p is pressure (cm Hg).

3. Computational procedures

Ab initio studies. Molecules of CO_2, the three alkanes (CH_4, CH_3CH_3, and $CH_3CH_2CH_3$), and three fluoroalkanes (CF_4, CH_3CF_3, and $CH_3CH_2CF_3$) were constructed using Spartan 5.1 (Wavefunction, Inc.). Their *Z*-matrix coordinates of each were imported to GAUSSIAN 94 running on a 12-processor (R-10010) SGI PowerChallengeXL server. Geometries were optimized (GAUSSIAN 94/Opt) using MP2/6-311++G^{**} and the polarizabilities, the dipole and quadrupole moments, and energies were obtained from single-point (MP2/6-311++G^{**}) calculations. The coordinates of the optimized structures were then exported to Spartan for calculation and display of the electrostatic potential distribution mapped on the electron density surface.

To form an equilibrated CO_2 complex with ethane, propane, trifluoroethane, or trifluoropropane, both molecules were constructed and the energy of the system consisting of CO_2 and the alkane or fluoroalkane was minimized by means of Insight II (Accelrys) using the COMPASS force field. The complex or dimer was further optimized using HF/3-21G^* in Spartan and then MP2/6–311++G^{**} in GAUSSIAN94. Electrostatic potentials of the dimers were then obtained by means of Spartan for comparison with the unpaired molecules.

Molecular simulation. Chains of PTFEP with 120 and 150 repeat units were prepared using an initial *cis–trans* conformation. The COMPASS force field described earlier and the charge group method for electrostatic interactions were used. For PTFEP, the neutral charge groups were $NP(OCH_2)_2$ and CF_3. The polymer chain was then minimized for 1000 steps and used to construct a periodic amorphous cell using the explicit image convention. Based on a conventional RIS model, a stepwise chain construction scheme using the torsional potential obtained from COMPASS was used to generate the initial structure. Five different cells were prepared for both the 120 and 150-repeat unit cells. Additional details of the computational procedures are given elsewhere [32].

A 100-step minimization process was used to refine the resulting cells and eliminate any bad contacts (overlapping or close contacts of atoms). This was followed by an annealing procedure during which the periodic cell was heated from 300 to 600 K at intervals of 50 K and then cooled back to 298 K. At each step of the cycle, the cells were subject to 50-ps NPT dynamics. Next, 50-ps NVT dynamics was used to further relax the polymer structure with the cell density fixed at the average value obtained from previous 50 ps of NPT dynamics. This was followed by additional 150 ps of NPT dynamics. The first 50 ps of dynamics were discarded while the remaining 100 ps was saved as a history file.

The polymer cells with smallest energy and density variation during the final NPT dynamics run was selected from each set of five cells for GCMC simulation of

Table 2
Results of MP2/6-311++G** calculations

Compound	μ (D)	Θ (D Å)	MP2 energy (a.u.)[a]	α (Å^3)
CO_2	0	−4.62	−188.21	15.37
CH_4	0	0	−40.38	14.04
CF_4	0	0	−436.72	16.08
CH_3CH_3	0	−0.74	−79.57	25.89
CH_3CF_3	2.75	3.56	−376.84	26.59
$CH_3CH_2CH_3$	0.086	0.54	−118.77	37.98
$CH_3CH_2CF_3$	2.86	−0.76	−416.03	38.27

[a] 1 a.u. = 627.5095 kcal mol^{-1} = 2629 kJ mol^{-1}.

solubility at 298 K. The dimensions of the cell chosen from among the 120-r.u. cells was 30.9 Å; the 150-r.u. cell was slightly bigger at 32.9 Å. Based on studies of Wagner and co-workers [33,34], these box sizes are sufficiently large that simulation results for solubility should be reliable. Gas (He, N_2, O_2, CH_4, CO_2, or Xe) concentrations were determined at pressure increments of 0.5 atm over a range from 0 to 5 atm. A total of 200,000 steps were used for each sorption measurement (pressure and gas).

For PCF analysis of CO_2 interatomic interactions, four CO_2 molecules were inserted in an amorphous cell of PTFEP in such a manner that the distance between any two CO_2 molecules was more than half of the cell length. Next, 2 ns of NVT dynamics were run using the Anderson [35] temperature control algorithm, a 1.0 Å spline width, and a 12 Å cutoff for nonbonded interactions. Trajectory files were recorded at intervals of 1 ps. PCFs were calculated from 1 ns trajectories over 1.5 ns of NPT dynamics at 300 K. Van der Waals radii were obtained from the 6–9 Lennard–Jones expression used by COMPASS. For analysis of PCF distributions, trajectory frames were loaded into memory and different functional groups were assigned as subsets. PCF distributions for different CO_2-functional group pairs were obtained by the Amorphous_Cell/Analysis module of InsightII. The average PCF for CO_2 with different atoms of PTFEP was calculated as

$$g_i(r) = \frac{N_i(r)}{\rho_i N_{CO_2} N_S 4\pi r^2 \, dr} \quad (10)$$

where $N_i(r)$ is the number of atoms of type i in a spherical shell between r and $r + dr$, ρ_i is the bulk density of atoms of type i in PTFEP, N_S is the total number of frames used for the analysis, and N_{CO_2} is the number of CO_2 molecules.

4. Results and discussion

Ab initio studies. As shown by values in Table 2, MP2/6-311++G** calculations yield a value of −4.62 D Å for the quadrupole of CO_2. This compares favorably with the established experimental value of −4.3 D Å [21]. Dehommelle et al. [36] reported a value of −4.13 D Å from MP2/VDJ calculations. Glaser et al. [29] have compared values using different basis sets at the RH, MP2, and QCISD(fc) levels of theory. At MP2/6-311 + G*, their value for the quadrupole is −4.59 D Å which is very close to the value of −4.62 obtained in this study for MP2/6-311++G**. In their study, a value of −4.28 D Å was obtained at the very highest computational level of QCISD/cc-pVTZ +. As shown by values given in Table 2, only CH_3CF_3 and $CH_3CH_2CF_3$ have appreciable dipole moments; CH_4 and CF_4 have neither dipole nor quadrupole moments. As shown by values given in Table 2, there are no significant differences in polarizabilities between the flourinated and nonfluorinated alkanes.

As shown in Fig. 3, dimer orientations indicate clear association between the carbon of CO_2 and the fluorine atoms of CF_4, CH_3CF_3, and $CH_3CH_2CF_3$. Interaction energies were calculated as the difference between the total energy of the CO_2–alkane or CO_2–fluoroalkane dimer and the sum of the energies of CO_2 and the alkane or fluoroalkane (Table 2). As shown in Table 3, interaction energies between CO_2 and the fluoroalkanes are approximately twice the magnitude of the corresponding CO_2–alkane interactions. The strongest interactions occur between CO_2 and CH_3CF_3 and particularly between CO_2 and $CH_3CH_2CF_3$ for which there is a significant dipole–quadrupole interaction. Interaction energies for CO_2–CF_3CH_3 and CO_2–$CF_3CH_2CH_3$ are −8.92 and −11.5 kJ mol^{-1}, respectively. In the case of CO_2–$CF_3CH_2CH_3$, approximately half of the total interaction energy is due to dipole–quadrupole interaction. It is noted that the interaction energy between CO_2 and propane is smaller (−6.88 kJ mol^{-1}) but not

Table 3
MP2/6-311++G** energies of CO_2 dimers

Dimer	R (Å)	Total energy (a.u.)	Interaction energy	$U_{\mu\Theta}$	$U_{\Theta\Theta}$	Other[a]
CO_2–CH_4	3.52	−228.59	−3.14	0	0	−3.14
CO_2–CF_4	3.84	−624.93	−6.04	0	0	−6.04
CO_2–CH_3CH_3	3.54	−267.78	−5.17	0	0	−5.17
CO_2–CF_3CH_3	3.96	−565.05	−8.92	−2.12	0.617	−7.42
CO_2–$CF_3CH_2CH_3$	3.57	−306.98	−6.88	0	0	−6.88
CO_2–$CF_3CH_2CH_3$	3.73	−604.25	−11.5	−6.01	−1.34	−4.11

Unless otherwise indicated, units are kJ mol^{-1}.
[a] Dispersion, induction, and electrostatic (other than dipole and quadrupole terms).

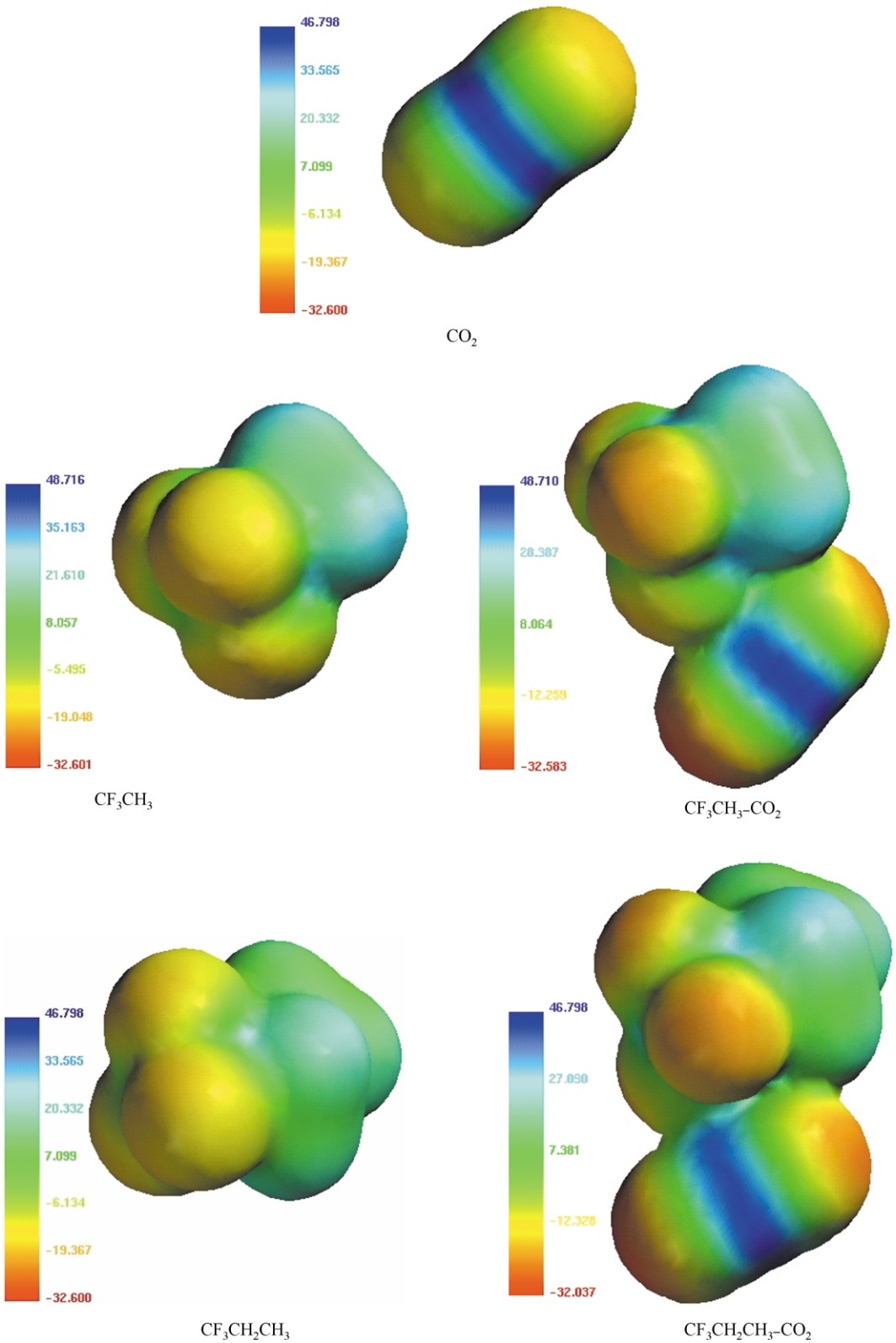

Fig. 4. Mapping of electrostatic distribution on the electron density surfaces of CO_2, CF_3CH_3, $CF_3CH_3-CO_2$, $CH_3CH_2CF_3$, and $CH_3CH_2CF_3-CO_2$. Red regions indicate areas of high electronegativity; blue regions indicate areas of high positive charge.

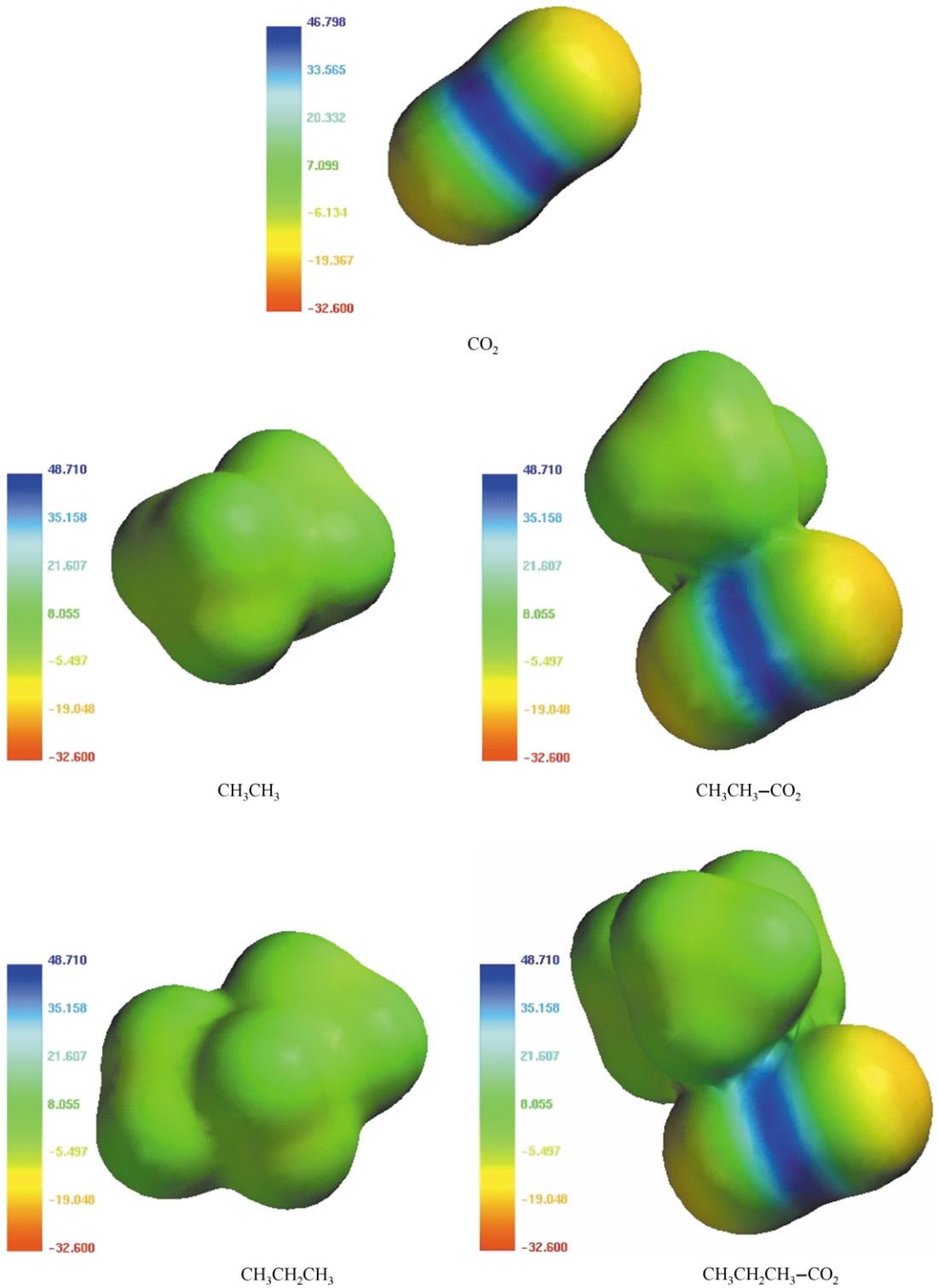

Fig. 5. Mapping of electrostatic distribution on the electron density surfaces of CO_2, CH_3CH_3, $CH_3CH_3-CO_2$, $CH_3CH_2CH_3$, and $CH_3CH_2CH_3-CO_2$.

negligible in the absence of a dipole–quadrupole interaction and may be attributed to dispersion and other interactions [36].

It should be noted that the magnitudes of the interaction energies for $CO_2-CF_3CH_3$ and $CO_2-CF_3CH_2CH_3$ lie below the range typically reported for hydrogen bonding (i.e. 12–30 kJ mol^{-1}) [30] but are larger than observed for CO_2 and poly(methyl methacrylate) (PMMA). PMMA also exhibits high CO_2 permselectivity as shown in Fig. 1 and has been reported to exhibit elevated CO_2 solubility [11]. From FTIR measurements, Kazarian et al. [37] obtained a

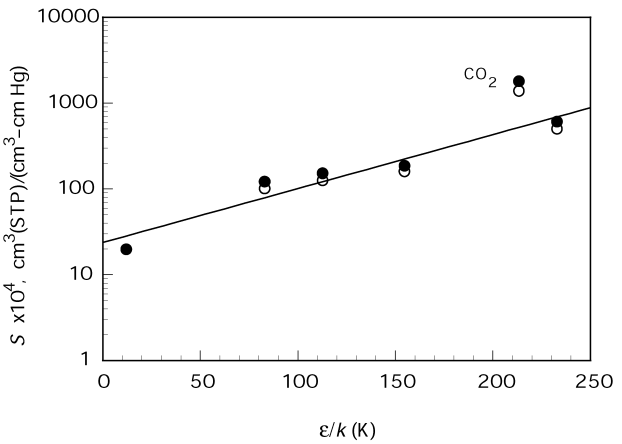

Fig. 6. Semilogarithmic plot of gas solubility obtained at 298 K from GCMC simulation of a 120-repeat unit (○) and 150-repeat unit cell (●) versus the Lennard–Jones potential well-depth parameters, ε/k, of He, N_2, O_2, CH_4, CO_2, and Xe. Lennard–Jones potential well-depth parameters were taken from Teplyakov and Meares [20]. The line represents the least-square fit ($R^2 = 0.9320$) of simulation data for the 150 repeat unit cell with the exclusion of the CO_2 data point.

value of 4.2 kJ mol^{-1} that they attributed to a Lewis acid–base interaction of CO_2 with the carbonyl group of PMMA.

Electrostatic potentials are mapped onto the electron density surfaces of CO_2, CH_3CF_3, and $CH_3CH_2CF_3$ in Fig. 4. Comparison with the electrostatic potentials for the CO_2–CF_3CH_3 and CO_2–$CF_3CH_2CH_3$ dimers indicate the appearance of a reddish orange coloration at the tops of the fluorine atoms of the fluoroalkanes and the oxygens atoms of CO_2. The prominence of red coloration is somewhat more intense for the oxygen closest to the fluorine atoms. These visual indications of electron redistribution are evident in small changes in the ESP charges as well. For example, ESP charges on fluorine decreases from −0.26 for CH_3CF_3 to −0.29 for CO_2–CF_3CH_3 and from −0.28 for $CH_3CH_2CF_3$ to −0.29 for CO_2–$CF_3CH_2CH_3$. In the case of CO_2, the ESP charge of the oxygen atom closest to fluorine decreases from −0.439 to −0.465 for CO_2–CH_3CF_3 and from −0.439 to −0.468 for CO_2–$CF_3CH_2CH_3$. As shown in Fig. 5, this small change in electron distribution for the oxygen sites of CO_2 does not occur in the case of the alkane dimers. For CO_2–CH_3CH_3, the ESP charges for both oxygen atoms of CO_2 are equal and only change from −0.439 to −0.445 and from −0.439 to −0.445 for CO_2–$CH_3CH_2CH_3$.

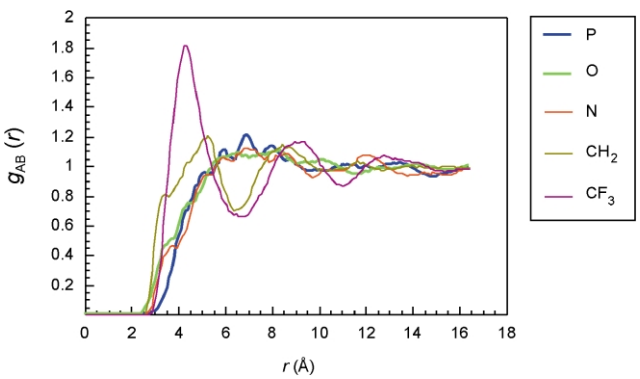

Fig. 7. Plot of the pair correlation function, $g_{AB}(r)$, versus the separation distance, r (Å), between CO_2 and the phosphorus and nitrogen atoms along the chain backbone and between CO_2 and the oxygen atoms, methylene groups, and trifluoromethyl groups of the trifluoroethoxy side chains of PTFEP.

Molecular simulations. As shown in Fig. 6, gas solubility coefficients obtained from GCMC simulations at 298 K follow closely the correlation given by Eq. (3) with the exception of the CO_2 solubility which lies above the correlation relationship as previously shown from permeability data for PTFEP and two other fluorine-containing polymers in Fig. 2. The line representing a least-squares fit ($R^2 = 0.9320$) of the five data points (excluding CO_2) obtained for the 150-r.u. periodic cell (32.9 Å) has a slope of 3.3×10^{-2} K^{-1} which is consistent with data for other polymers. As shown in Fig. 6, sorption data for a slightly smaller (30.9 Å) cell obtained by building an amorphous cell from a 120-r.u. cell indicate good reproducibility of the results. There is also good qualitative agreement with the experimental data for a semicrystalline (60%) sample [14] as was shown in Fig. 2; however, solubility values for the semicrystalline samples are smaller than obtained for the amorphous state of the simulation as would be expected. As will be reported in a subsequent report [38], GCMC simulation of the crystalline forms of PTFEP confirm that gas solubility is negligible in comparison with the amorphous state.

In Fig. 7, averaged pair correlation functions are plotted against separation distance for the phosphorus and nitrogen atoms along the backbone of PTFEP and for the CH_2 and CF_3 groups and the oxygen atoms in the side chains. In the case of polydimethylphosphazene, Gallazzi et al. [39] have suggested that the lone pair electrons of the nitrogen atom along the polymer backbone could participate in donor–acceptor interaction with carbon dioxide; however, the results for N in the case of PTFEP do not indicate any preferential interaction of CO_2 with nitrogen. As shown in Fig. 7, association is the strongest for CO_2 with CF_3 and second strongest for CO_2 with the CH_2 group that is attached directly to CF_3. These MD results are consistent with the previously discussed ab initio calculations that indicate a specific (i.e. dipole–quadrupole) interaction between CO_2 and the CF_3 group of trifluoroethane or trifluoropropane. The separation between CO_2 and the CF_3 group of PTFEP at the maximum of the PCF is approximately 4.3 Å which is only slightly larger than the ab initio results for CO_2 and the fluoroalkanes in Fig. 3(b) and (c). The sharpness of the peak for CO_2–CF_3 appearing in the PCF plot of Fig. 7 is a strong evidence for preferential association of CO_2 with the trifluoroethoxy group of PTFEP.

5. Conclusions

Results of ab initio (MP2/6-311++G**) calculations indicate favorable interaction between CO_2 and the polar fluoromethyl group of trifluoroethane and trifluoropropane. Analysis of the data suggests that quadrupole–dipole interaction is an important contribution to the total energy of interaction. These conclusions of specific association are consistent with results of GCMC simulation of solubility and molecular dynamics simulation of pair correlations of CO_2 with the trifluoromethyl group of PTFEP. Preferential association of CO_2 may occur on a similar basis of quadrupole–dipole interaction with the accessible fluorine sites of other polymers such as PTFPMS that also exhibit high CO_2 solubility. It is clear from the ab initio and molecular dynamics simulations reported in the present study that close physical association (less than 4.3 Å between centers of mass) is necessary. For some polymers with bulky groups, perhaps including 6F polyimides and related polymers (see Table 1), such close contacts may not be possible and other contributions such as increased free volume due to steric repulsions may lead to high solubility and permselectivity.

Acknowledgements

Major support from the Ohio Board of Regents (Investment Fund) for computer facilities and software used in these studies is greatly appreciated. This material is based partially upon work supported by the National Science Foundation under Grant no. 9810320.

References

[1] Yee GG, Fulton JL, Smith RD. J Phys Chem 1992;96:6172–81.
[2] Dardin A, DeSimone JM, Samulski ET. J Phys Chem B 1998;102:1775–80.
[3] Dinoia TP, Conway SE, Lim JS, McHugh MA. J Polym Sci, Part B: Polym Phys 2000;38:2832–40.
[4] Tuminello WH, Dee GT, McHugh MA. Macromolecules 1995;28:1506–10.
[5] Shah VM, Hardy BJ, Stern SA. J Polym Sci, Part B: Polym Phys 1986;24:2033–47.
[6] Stern SA, Shah VM, Hardy BJ. J Polym Sci, Part B: Polym Phys 1987;25:1263–98.
[7] Hellums MW, Koros WJ, Husk GR, Paul DR. J Membr Sci 1989;46:93–112.
[8] Kim T-H, Koros WJ, Husk GR. Sep Sci Technol 1988;23:1611–26.
[9] Tanaka K, Kita H, Okano M, Okamoto K-I. Polymer 1992;33:585–92.
[10] El-Hibri MJ, Paul DR. J Appl Polym Sci 1986;31:2533–60.
[11] Chiou JS, Paul DR. J Appl Polym Sci 1986;32:4793–814.
[12] Masuda T, Iguchi Y, Tang B-Z, Higashimura T. Polymer 1988;29:2041–9.
[13] Yampol'skii YP, Bespalova NB, Finkel'shtein ESh, Bondar VI, Popov AV. Macromolecules 1994;27:2872–8.
[14] Hirose T, Kamiya Y, Mizoguchi K. J Appl Polym Sci 1989;38:809–20.
[15] Robeson LM. J Membr Sci 1991;62:165–85.
[16] Kajiwara M. Sep Sci Technol 1991;26:841–52.
[17] Starannikova LE, Tür DR, Teplyakov VV, Platé NA. Polym Sci 1994;36:1906–11.
[18] von Amerongen GJ. Rubber Chem Technol 1964;37:1065–152.
[19] Toi K, Morel G, Paul DR. J Appl Polym Sci 1982;27:1997–2005.
[20] Teplyakov V, Meares P. Gas Sep Purif 1990;4:66–74.
[21] Buckingham AD, Disch RL. Proc R Soc A 1963;273:275–89.
[22] Møller C, Plesset MS. Phys Rev 1934;46:618–22.
[23] Sun H. J Phys Chem B 1998;102:7338–64.
[24] Sun H, Ren P, Fried JR. Comput Theor Polym Sci 1998;8:229–46.
[25] Sun H. Macromolecules 1995;28:701–12.
[26] Yang J, Ren Y, Tian An-m, Sun H. J Phys Chem B 2000;104:4951–7.
[27] Fried JR, Ren P. Comput Theor Polym Sci 1999;9:111–6.
[28] Fried JR, Ren P. Comput Theor Polym Sci 2000;10:447–63.
[29] Glaser R, Wu Z, Lewis M. J Mol Struct 2000;556:131–41.
[30] Rigby M, Smith EB, Wakeham WA, Maitland GC. The forces between molecules. Oxford: Oxford University Press; 1986.
[31] Metropolis N, Rosenbluth AW, Rosenbluth MN, Teller AH, Teller E. J Chem Phys 1953;21:1087–92.
[32] Hu N. PhD Dissertation. University of Cincinnati; 2003.
[33] Cuthbert TR, Wagner NJ, Paulaitis ME. Macromolecules 1997;30:3058–65.
[34] Cuthbert TR, Wagner NJ, Paulaitis ME, Murgin HG, D'Aguanno B. Macromolecules 1999;32:5017–28.
[35] Andrea TA, Swope WC, Andersen HC. J Chem Phys 1983;79:4576–84.
[36] Delhommelle J, Grannucci G, Brenner V, Millie P, Boutin A, Fuchs AH. Mol Phys 1999;97:1117–28.
[37] Kazarian SG, Vincent MF, Bright FV, Liotta CL, Eckert CA. J Am Chem Soc 1996;118:1729–36.
[38] Fried JR, Hu N. Submitted for publication.
[39] Gallazzi MC, Montoneri E, Savarino P, Bianchi F, Di Landro L. J Mater Sci Lett 1993;12:436–8.